International Journal of Remote Sensing, 2014
Vol. 35, Nos. 11–12, 4086–4098, http://dx.doi.org/10.1080/01431161.2014.916453

Generation sites of internal solitary waves in the southern Taiwan Strait revealed by MODIS true-colour image observations

Xiaolin Bai[a], Zhiyu Liu[a]*, Xiaofeng Li[b], and Jianyu Hu[a]

[a]*State Key Laboratory of Marine Environmental Science and Department of Physical Oceanography, College of Ocean & Earth Sciences, Xiamen University, Xiamen 361005, China;* [b]*GST, NESDIS, NOAA, College Park, MD 20746, USA*

(*Received 22 September 2013; accepted 26 December 2013*)

Based on 12 years (2000–2011) of Moderate Resolution Imaging Spectroradiometer (MODIS) true-colour images, statistical characteristics of internal solitary waves (ISWs) in the southern Taiwan Strait were studied. Two types of ISWs with a distinct scale of wave crest length and geographic distributions were identified: Type-I waves have larger wave crest lengths and span a large area from the southern Taiwan Strait to the northern South China Sea, while Type-II waves have smaller wave crest lengths and appear only at the southeastern corner of the Taiwan Strait. Further analyses based on an empirical model of ISW propagation and on the calculations of the depth-integrated internal tide-generating body force suggested that Type-I waves mainly originate from the Luzon Strait, while Type-II waves are locally generated at the shelf break in the southeastern corner of the Taiwan Strait.

1. Introduction

Internal solitary waves (ISWs) are ubiquitous features in oceans, fjords, and lakes (Gerkema and Zimmerman 2008). They can propagate over several hundreds of kilometres, produce strong turbulence and mixing with a considerable velocity shear, and modify thermohaline structures of the water column (Gerkema and Zimmerman 2008; Alford et al. 2011; Guo and Chen 2014).

Although representing ocean interior motion, ISWs have visible manifestations at the surface, which are often captured by satellite images (Mitnik et al. 2000; Bakhanov and Ostrovsky 2002). For instance, synthetic aperture radar (SAR) is widely used for studying ISWs owing to its considerable advantages of not being affected by meteorological conditions and its very high resolution (Mitnik et al. 2000; Zhao et al. 2004; Zheng et al. 2007). Based on sea surface roughness in sunglint area, these waves can also be imaged on high-resolution optical imagery (Apel et al. 1985), such as Satellite Pour l'Observation de la Terre (SPOT) (Mitnik et al. 2000). In addition, the chlorophyll images derived from ocean colour measurements of the Seaviewing Wide Field-of-view Sensor (SeaWiFS) and Moderate Resolution Imaging Spectroradiometer (MODIS) have also been successfully employed in the study of ISWs (da Silva et al. 2002; Vázquez et al. 2009; Pan et al. 2012; Muacho et al. 2013). However, the application of ocean colour images in studying ISWs is severely limited by their relatively low resolution (1.1 km) and, in some cases, by the interference of upwelling signatures at the ocean surface. In comparison, the resolution of MODIS true-colour images is higher (250 m), which is suitable for detecting

*Corresponding author. Email: zyliu@xmu.edu.cn

ISWs, as demonstrated by Jackson (2007) in a study of the global distributions of ISW occurrence.

The northern South China Sea (SCS) is one of the predominant regions of the world's oceans where energetic ISWs occur frequently (e.g. Guo and Chen 2014). The characteristics and dynamics of ISWs have been studied based on *in situ* observations at a variety of locations in the northern SCS (Apel et al. 1997; Klymak et al. 2011; Fu et al. 2012; Guo et al. 2012). Their geographic distributions have been revealed by analysis of SAR as well as MODIS true-colour images (Zhao et al. 2004; Zheng et al. 2007; Li, Zhao, and Pichel 2008; Li, Jackson, and Pichel 2013). The Taiwan Strait (TS) is a shallow (average depth of about 60 m) channel connecting the SCS and the East China Sea. It lies to the northeast of the SCS, and is a region with ISWs frequently occurring in its southern part (Bai et al. 2013). Some basic features of these ISWs have been described based on *in situ* time-series measurements of temperature and salinity (Bai et al. 2013), but the spatial distributions and temporal variations, as well as generation mechanisms and generation sites of the ISWs, are still largely unknown. Although ISWs in the southern TS are commonly thought to originate from the Luzon Strait (e.g. Zheng et al. 2007; Li, Zhao, and Pichel 2008; Guo and Chen 2014), their local generation at the shelf break in the southeastern corner of the TS will be shown to play an important role.

In this study, we investigate the statistical characteristics of the ISWs in the southern TS using 12 years (2000–2011) of MODIS true-colour images.

2. MODIS observations and analysis

2.1. *MODIS true-colour images*

The MODIS sensors are on board the National Aeronautics and Space Administration (NASA) satellites Terra and Aqua, which were launched on 18 December 1999 and 4 May 2002, respectively, and are still operational. Terra passes from north to south across the equator every morning, while Aqua passes from south to north over the equator every afternoon. Both can observe the entire Earth in one day. True-colour images are composites of data from three MODIS visible channels (i.e. red band centred at 645 nm, green band at 555 nm, and blue band at 469 nm). These true-colour images are produced from calibrated, corrected, and geo-located radiance (Level-1 B) data, with a spatial resolution of 250 m (Jackson 2007), and can be downloaded from NASA's LAADS (Level-1 and Atmosphere Archive and Distribution System) website (http://ladsweb.nascom.nasa.gov/index.html).

2.2. *Manifestation of ISWs in MODIS true-colour images*

Sunglint is the specular reflection of light from sea surface to the detector, and its relative strength is mainly determined by sea surface roughness (Wald and Monget 1983). ISWs induce divergence and convergence of sea surface currents as they propagate, which modify the sea surface roughness and thus are visible in MODIS true-colour images if they are in a sunglint area. In the images, the smooth front zone (due to surface current divergence) appears as a bright band, while the rough front zone (due to surface current convergence) appears as a dark band, because a smooth surface can reflect more light to the sensor than a rough surface. Therefore, ISWs are manifested as alternate bright and dark bands in MODIS true-colour images (see Figure 5 in Liu et al. 1998 for a schematic diagram). Examples are shown in Figure 1.

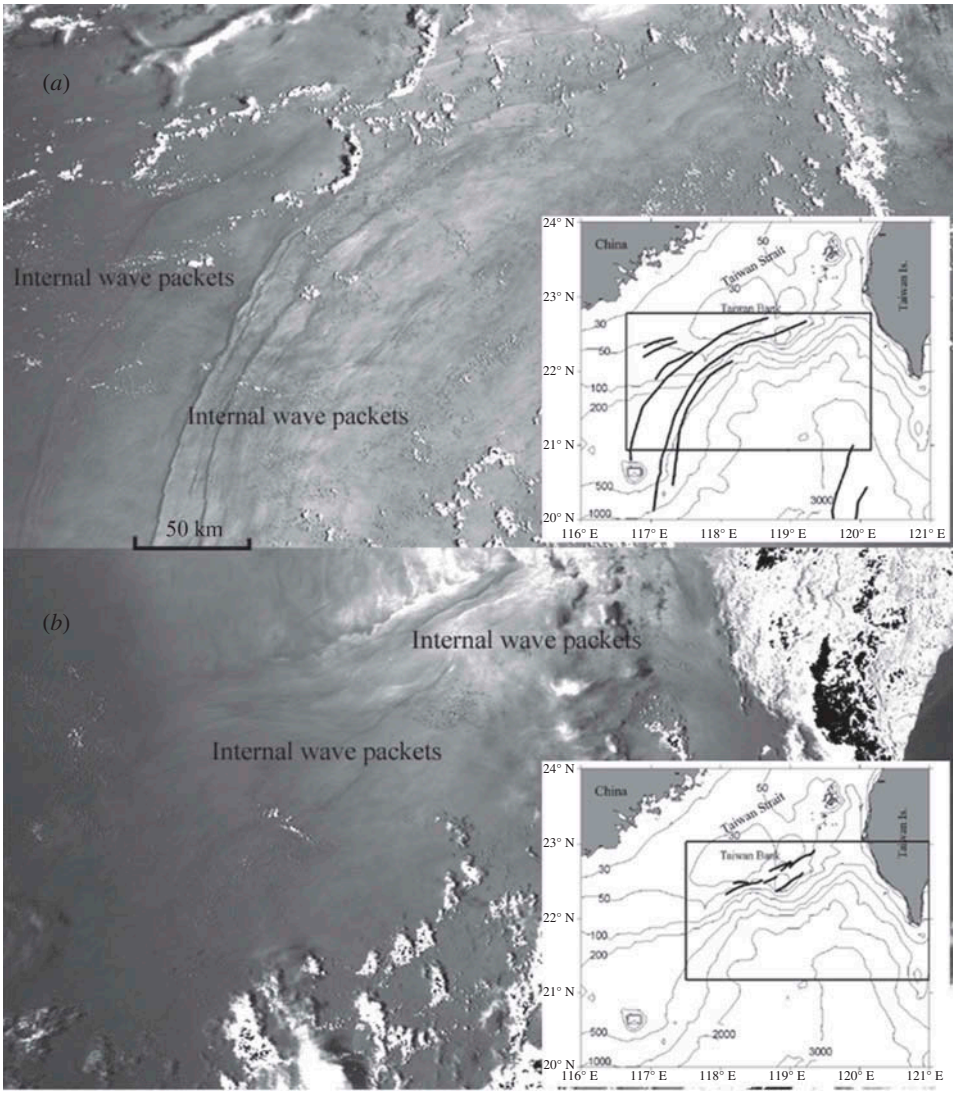

Figure 1. MODIS true-colour images of the southern Taiwan Strait and the northern South China Sea (*a*) at 02.55 UTC on 20 July 2008 and (*b*) at 05.15 UTC on 24 June 2007, respectively. The region covered by each image is denoted by a black box in the inserted maps. ISW packets visible in MODIS images are shown in the inserted maps as thick lines.

2.3. *Analysis of MODIS observations: two types of ISW in the southern TS*

To study the statistical characteristics of ISWs in the southern TS, we searched the entire MODIS archive for clear MODIS true-colour images. The images are selected only when ISWs were detected in the TS between 22° N and 24° N. As such, a total of 93 images were collected. These images cover a period of 12 years (2000–2011).

Figure 1 shows two typical MODIS true-colour images in the study region, acquired at 02.55 UTC on 20 July 2008 and 05.15 UTC on 24 June 2007. Identified ISW packets are labelled in the images. In general, ISW packets are divided into a single-wave packet containing only one ISW and a multiple-wave packet composed of a group of

rank-ordered waves (Zhao et al. 2004). For clarity of presentation, each ISW packet is indicated by the crest line of its leading wave (i.e. the only wave in a single-wave packet or the fastest wave in a multiple-wave packet).

As shown in the inserted map, the ISW crest lines in Figure 1(*a*) are much longer than those in Figure 1(*b*). The former extend from the southern TS to the northern SCS, while the latter locate only at the southeastern corner of the TS. In fact, out of the 93 images, 79 present features similar to Figure 1(*a*) while the other 14 present features similar to Figure 1(*b*). The distinct features in regard to the scale of wave crest length and geographic distributions are interesting and seem to suggest that there may be two different generation sites of the ISWs in the southern TS. We will examine this possibility and some statistical characteristics of these waves in the following sections. For clarity of presentation, we term the two types of wave as Type-I and Type-II. Type-I waves are those having a much larger wave crest length, and extend from the southern TS all the way to the northern SCS, while Type-II waves denote those with a much smaller wave crest length occurring only at the southeastern corner of the TS.

3. Generation sites of the ISWs

3.1. *Spatial distribution of MODIS-observed ISWs*

Two types of ISW were noted in an analysis of MODIS true-colour images. To illustrate this more clearly, the statistical distributions of ISWs in the southern TS based on all 93 images are shown in Figure 2.

As shown in Figure 2(*a*), the crest lines of Type-I waves are mainly distributed on the continental slope of the southern TS between 30 and 200 m isobaths. To the south of 22° N, the crest lines are mainly located to the west of 118° E, while a smaller number of crest lines are sparsely distributed to the east of 118° E. From the geographical distribution and the curvature of the crest lines in Figure 2(*a*), one can see a tendency where Type-I waves propagate westward and northwestward from the Luzon Strait to the continental slope areas.

As shown in Figure 2(*b*), Type-II waves are also mainly distributed between 30 and 200 m isobaths on the continental slope of the southern TS between 22° N and 23° N.

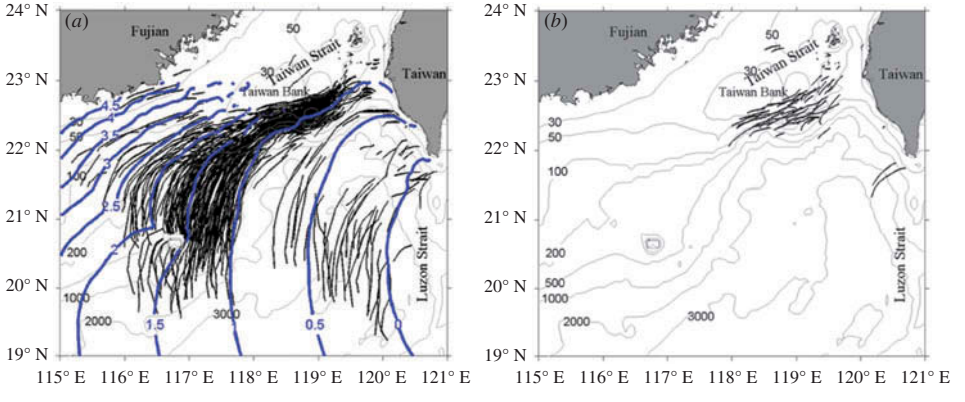

Figure 2. Distribution of ISWs in the southern Taiwan Strait and northern South China Sea revealed by MODIS true-colour images from 2000 to 2011 for (*a*) Type-I waves and (*b*) Type-II waves. The thin grey contours mark isobaths in metres. The thick blue contours show the arrival time of ISWs generated in the Luzon Strait, marked in days, according to an empirical model developed by Jackson (2009).

Given their geographic distribution shown in Figure 2(*b*), these ISWs were likely to have been generated locally rather than having been propagated from the Luzon Strait, because there were almost no ISWs observed between the Luzon Strait and the continental slope. To summarize, we speculate that these two types of ISW originate from two different sites: the Luzon Strait for Type-I waves and the shelf break at the southeastern corner of the TS for Type-II waves. Evidence for this will be explored in the following two sections.

3.2. *Evidence from an empirical model of ISW propagation*

To gain further evidence for the conjecture from spatial distributions of ISWs, we compare the observations by MODIS images to predictions from an empirical model. The empirical model was developed by Jackson (2009) to estimate ISW locations at a particular time after their generation in the Luzon Strait. It is based on a two-dimensional eikonal differential equation and a parameterized function of phase speed (Jackson 2009). In Figure 2(*a*), the blue contours, with an interval of half a day, represent the travel time of ISWs after their generation in the Luzon Strait. These represent the first arrival time of a propagating wave front; subsequent arrivals resulting from wave reflections have not been taken into account. Evidently, the model-predicted wave arrivals are highly consistent with MODIS observations of ISW locations, indicating that Type-I waves originate in the Luzon Strait.

The Luzon Strait has been commonly considered as the source of ISWs in the SCS (Zhao et al. 2004; Klymak et al. 2006; Zhao and Alford 2006; Zheng et al. 2007, 2008; Buijsman, Kanarska, and McWilliams 2010; Vlasenko, Guo, and Stashchuk 2012; Li, Zhao, and Pichel 2008, Li, Jackson, and Pichel 2013). In their propagation from deep water (deeper than 1000 m between 118–120° E) to the continental shelf, ISWs gradually evolve under the effects of nonlinear steepening of the continental slope (Djordjevic and Redekopp 1978; Zhao and Alford 2006). This is why ISWs are mainly distributed on the continental slope onshore of the 1000 m isobaths, but sparsely distributed between 118° E and the Luzon Strait (Figure 2(*a*)).

3.3. *Evidence from internal tide-generating body force calculations*

The generation sites of the ISWs can be further examined via analysing the distribution of internal tide-generating body force. According to Baines (1982), the depth-integrated body force F can be calculated as

$$F = -\frac{\vec{\boldsymbol{Q}}\nabla H}{\omega H^2}\int_{-H}^{0} zN^2(z)dz, \tag{1}$$

where ω is the tidal angular frequency (rad s^{-1}), z is the vertical coordinate ($z = 0$ at sea surface, upward positive), $N(z)$ is the local buoyancy frequency, $\boldsymbol{Q}$ is the barotropic tidal transport $\boldsymbol{Q} = (Q_x, Q_y) = (uH, vH)$, u and v are the zonal and meridional components of the barotropic tidal current, and H is the local water depth.

The spatial distribution of the body force F has been used to locate possible hot spots of internal wave generation in the world's oceans (Merrifield and Holloway 2002; Sherwin et al. 2002; Niwa and Hibiya 2004; da Silva, New, and Azevedo 2007; Magalhaes and da Silva 2012; Lozovatsky et al. 2012). For example, by analysing satellite images, Azevedo, da Silva, and New (2006) and da Silva, New, and Magalhaes (2009) showed that packets of nonlinear ISWs are often generated in regions where the value of F is large. Similarly, Li, Zhao, and Pichel (2008), Li *et al.* (2008) examined ISW

generation hot spots in the SCS and the East China Sea. Furthermore, $F > 0.25$ m^2 s^{-2} is usually regarded as a critical value for the generation of ISWs (Lozovatsky et al. 2012).

In the following, we calculate and analyse the internal tide-generating body force due to the M_2 tidal constituent in the northern SCS. The barotropic tidal transport data of the M_2 tide are obtained from the Oregon State University Tidal Inversion Software (OTIS 7.1, developed by Egbert and Erofeeva (2002)) at a horizontal resolution of 1/4°. The temperature and salinity profiling data, used for calculating the buoyancy frequency (N), are obtained from the Generalized Digital Environment Model database (GDEM-V 3.0) at a resolution of 1/2° (Carnes 2009), which is a monthly climatology dataset. We acquired bathymetry data from the five-minute gridded global relief database (ETOPO5). Both the velocity components and the calculated buoyancy frequency (N) are linearly interpolated onto finer grids with a resolution of 5 minutes. The maximum depth-integrated internal tide-generating body force over a complete tidal cycle is shown in Figures 3(*a*) and (*b*), corresponding to the cases shown in Figures 1(*a*) and (*b*), respectively.

As shown in Figure 3, two major hot spot regions ($F > 0.25$ m^2 s^{-2}) are located in the Luzon Strait and the continental slope near the southern TS. In regard to the case shown in

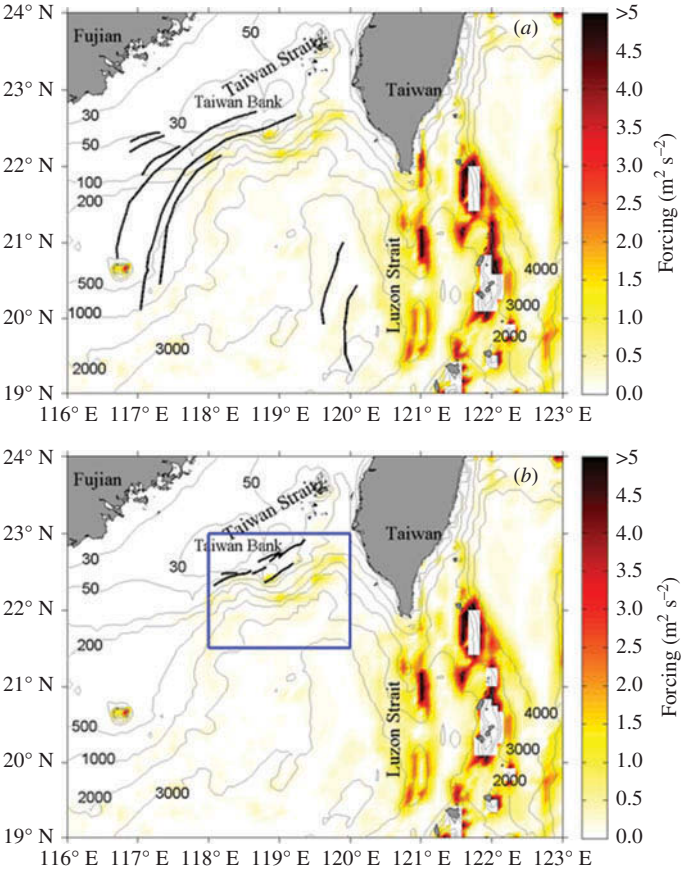

Figure 3. Map of the maximum depth-integrated internal tide-generating body force over a complete tidal cycle due to the M_2 tidal constituent for the study region using climatological buoyancy frequency (*a*) in July and (*b*) in June. ISWs are denoted by thicker black lines, corresponding to the cases in Figures 1(*a*) and (*b*). The thin grey contours show isobaths in metres.

Figure 3(*a*), the high-body force region is between 120.5° E and 122.5° E. Therefore, the groups of ISW (Type-I) are generated in the Luzon Strait. In Figure 3(*b*), although the value in the Luzon Strait is higher than that in the southeastern corner of the TS, we believe that the ISWs (Type-II) are primarily generated locally in the southeastern corner of the TS rather than in the Luzon Strait for the following two reasons. First, the hot spots are located along the isobaths between 200 and 500 m in the southern TS. ISWs can be generated due to the nonlinear steepening effect on the continental slope in this study area (Bai et al. 2013). Secondly, if the ISWs were generated from the internal tides originating from the Luzon Strait, one would also see ISWs on the continental slope of the northern SCS, where bathymetric conditions are also favourable for ISW generation (Lien et al. 2005). However, ISWs were only detected on the continental slope of the southern TS as shown in Figure 3(*b*). Therefore, calculations of the body force support the existence of the two generation sites, and indicate that the two types of ISW were generated from these sites.

4. Discussion

4.1. *Temporal variation in MODIS-observed ISWs*

In this section, we analyse the temporal variation in ISWs. Considering that stratification, which has a seasonal variation, is one of the most important conditions for generating ISWs, we focus on the monthly variation in ISW occurrence. The monthly MODIS-observed ISW occurrence frequency is defined as (Zheng et al. 2007)

$$p_{i(m)} = \frac{m_i}{A} \times 100\%, \tag{2}$$

where m_i is the number of the images in the ith month of the 12 years, and A is the number of total images. The monthly distributions of the two types of ISW are shown in Figure 4(*a*). As a whole, one can see that all 93 images are distributed from April to September. The high-occurrence frequencies are distributed in the summer months from June to August, reaching a peak of 38% in July, while fewer than 2% of the ISW images are observed in autumn, winter, and early spring. Although very different in absolute number of occurrences, there seems no evident difference in the relative frequency of

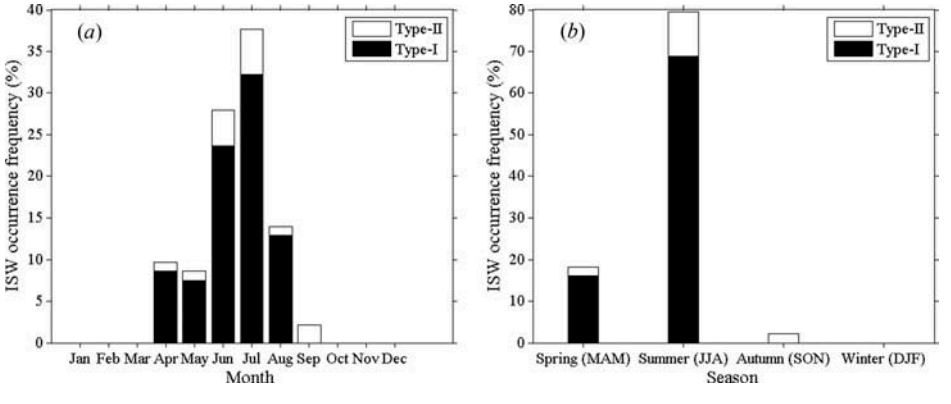

Figure 4. (*a*) Monthly and (*b*) seasonal distributions of MODIS-observed ISW occurrence in the southern Taiwan Strait.

occurrence between the two types of ISW. As shown in Figure 4(*b*), there is a pronounced seasonal variation in occurrence, with 18% in spring (MAM), the maximum frequency of 80% in summer (JJA), 2% in autumn (SON), and almost none in winter (DJF). However, it should be noted that this observation does not mean that ISWs do not occur in these winter months in the southern TS. Further discussions on this issue will be presented in Section 4.2.

Similarly, given the close relationship between the generation of ISWs and barotropic tidal currents (e.g. Zhao and Alford 2006; Zheng et al. 2007; Du, Tseng, and Yan 2008; Vlasenko, Guo, and Stashchuk 2012), we analyse the daily ISW occurrence frequency in a lunar month, defined as

$$p_{i(d)} = \frac{d_i}{A} \times 100\%, \tag{3}$$

where d_i is the number of images on the ith lunar day (i.e. the ith day in a lunar month). A lunar month is the time between two successive similar syzygies (new moon or full moon). Correspondingly, spring tide occurs from the 1st to 3rd and from the 15th to 18th lunar day, while neap tide occurs one week after the preceding spring tide. The statistical results are shown in Figure 5. Collectively, the high occurrence frequencies are distributed from the 1st to 8th lunar day and from the 17th to 23rd lunar day. About 37% of the images were collected during the first 8 days, with 33% from the 17th to 23rd lunar day. For Type-I waves, the lunar daily distributions are similar to the results of Du, Tseng, and Yan (2008), who found high ISW occurrence frequency from the 2nd to 6th, the 16th to 21st, and the 29th to 30th lunar day in the Luzon Strait. The lag of a few days in our statistical results is mainly due to the propagation time (about 1.5 days as shown in Figure 2(*a*)) from the Luzon Strait to the southern TS. On the other hand, because there were only 14 images collected for Type-II waves, it is difficult to identify a relationship between their occurrence and barotropic tidal currents. The low occurrence of Type-II

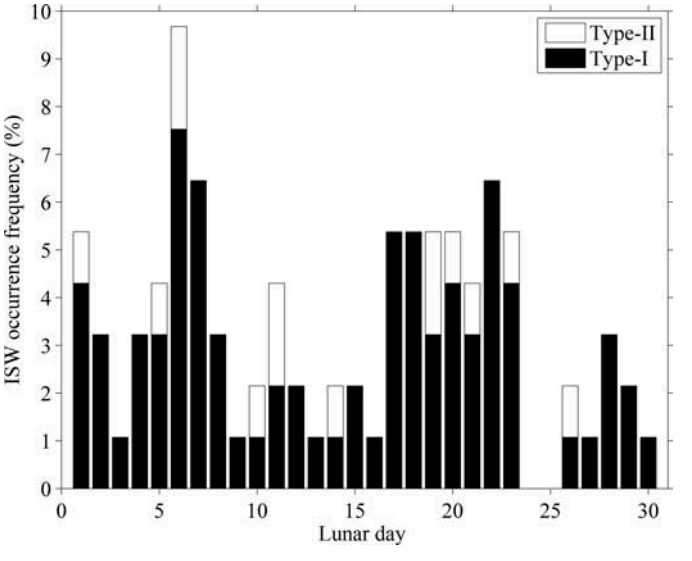

Figure 5. Lunar daily distribution of MODIS-observed ISW occurrence in the Taiwan Strait.

waves is presumably mainly due to their short lifespan; this is about 0.5 days over the continental slope of the southern TS as estimated from Figure 2(*a*), which is shorter than the cycling period of MODIS sensors (about 1 day). This obviously poses a challenge for the observation of Type-II waves: compared with Type-I waves, a much higher sampling frequency is required to capture their detailed characteristics and propagation features. *In situ* mooring-based observations have to be resorted to for this purpose, and it is a focus of our further studies.

4.2. *The applicability of MODIS in detecting ISWs*

In this study, the true-colour images were based on measurements of MODIS sensors on board both Aqua and Terra satellites. The detection of ISWs with MODIS imagery is affected by cloud cover. In fact, only 93 out of an available 11,129 images from NASA's Level 1 and Atmosphere Archive and Distribution System (LAADS) Web over the 12-year period (2000–2011) are cloud free and contain clear ISW signatures. In winter and spring, cloud cover in this region is almost 100%. Therefore, the statistical results shown in Figure 4 do not necessarily mean that there were no ISWs located in the southern TS during these seasons. To examine their possible existence for each season, we calculated the depth-integrated internal tide-generating body force for four seasons using high-resolution bathymetry data (a spatially filtered version for local bathymetry combining the survey data and ETOPO2v2 as employed in Jiang et al. 2011) and seasonal stratification profiles. As it is known that ISWs are generated in the Luzon Strait in all seasons (Zheng et al. 2007), in Figure 6 we only show results in the local generation region of the southern TS. It is evident that the hot spot band of internal tide

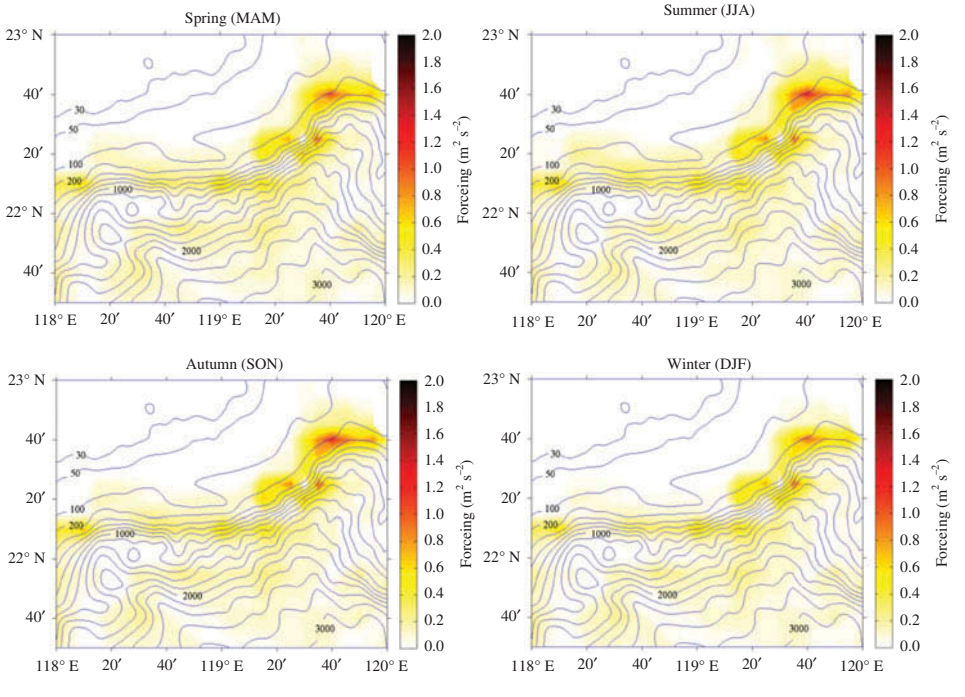

Figure 6. Map of the maximum depth-integrated internal tide-generating body force over a complete tidal cycle due to the M_2 constituent for the four seasons in the region shown with a blue box in Figure 3(*b*). The contours show isobaths in metres.

generation exists in the continental slope throughout all seasons, with a maximum value near 22.6° N, 119.7° E. Although the calculations show that the F value is relatively lower in spring and winter and higher in summer and autumn, it is sufficient (all >1 $m^2 s^{-2}$) for the generation of internal tides and ISWs (Lozovatsky et al. 2012). This suggests that ISWs may be generated during all seasons.

However, compared to other sensors, such as SPOT and SAR with a swath width of 60–100 and 500 km, respectively, the key advantage of MODIS imagery is its much larger swath width (2300 km) and more frequent revisiting coverage. Critical to this study, its swath width is large enough to cover both the southern TS and the northern SCS in one image, allowing one to distinguish the scales of wave crest length of ISWs over the whole study region. In addition, the statistical results presented in this study are valuable for planning future *in situ* and SAR observations (which are not affected by cloud cover) for a more robust statistical analysis.

5. Conclusion

In this paper, we investigated the statistical characteristics and generation sites of ISWs in the southern TS using MODIS true-colour images over a period of 12 years (2000–2011). Out of the collected 93 images, 79 show ISWs spanning a large area from the southern TS to the northern SCS; while the other 14 show ISWs located only at the southeastern corner of the TS. These distinct features of wave crest length and geographic distribution led us to speculate that ISWs may originate from two different generation sites. The conjecture was then tested and confirmed. The high consistency of the observed ISW propagations and the predictions of an empirical model support the hypothesis that Type-I waves mainly originate from the Luzon Strait, and the local generation of Type-II waves is supported by horizontal distribution of the depth-integrated internal tide-generating body force. Temporal variation in ISWs was analysed, and it was found that the occurrence of the two types of ISW has a possible seasonal variability with the maximum frequency in summer (80%) and the minimum in autumn and winter (about 2%). The lunar daily occurrence frequency of Type-I waves shows a similar feature to those in the Luzon Strait (e.g. Du, Tseng, and Yan 2008), but with a lag of about 1.5 days due to the propagation time from the Luzon Strait to the southern TS. However, calculations of depth-integrated body force using the climatology dataset suggest that ISWs may be generated in all seasons. These results imply that temporal variation requires further study, such as combing *in situ* with SAR observations, to examine whether ISWs occur in winter and show a seasonal variability, and to identify the link between the occurrence of Type-II waves and barotropic tidal currents.

Acknowledgements

The authors would like to thank NASA's LAADS Web for providing MODIS true-colour images. We would like to acknowledge Jiawei Chen for help with MODIS image processing. Meanwhile, we also appreciate valuable discussions with Quanan Zheng, J. C. B. da Silva, and C. R. Jackson. Constructive comments from three anonymous reviewers are also appreciated. The views, opinions, and findings contained in this report are those of the authors and should not be construed as an official NOAA or US government position, policy, or decision.

Funding

This work was supported by the National Natural Science Foundation of China (41006017, 41276006, and 41121091), the Fundamental Research Funds for the Central Universities of China (2010121030), and the National Basic Research Programme of China (2009CB21208).

References

Alford, M. H., J. A. MacKinnon, J. D. Nash, H. Simmons, A. Pickering, J. M. Klymak, R. Pinkel, O. Sun, L. Rainville, R. Musgrave, T. Beitzel, K. H. Fu, and C. W. Lu. 2011. "Energy Flux and Dissipation in Luzon Strait: Two Tales of Two Ridges." *Journal of Physical Oceanography* 41: 2211–2222. doi:10.1175/JPO-D-11-073.1.

Apel, J. R., M. Badiey, C. S. Chiu, S. Finette, R. Headrick, J. Kemp, J. F. Lynch, A. Newhall, M. H. Orr, B. H. Pasewark, D. Tielbuerger, A. Turgut, K. von der Heydt, and S. Wolf. 1997. "An Overview of the 1995 SWARM Shallow-Water Internal Wave Acoustic Scattering Experiment." *IEEE Journal of Oceanic Engineering* 22: 465–500. doi:10.1109/48.611138.

Apel, J. R., J. R. Holbrook, A. K. Liu, and J. J. Tsai. 1985. "The Sulu Sea Internal Soliton Experiment." *Journal of Physical Oceanography* 15: 1625–1651. doi:10.1175/1520-0485(1985)015<1625:TSSISE>2.0.CO;2.

Azevedo, A., J. C. B. da Silva, and A. L. New. 2006. "On the Generation and Propagation of Internal Solitary Waves in the Southern Bay of Biscay." *Deep Sea Research Part I: Oceanographic Research Papers* 53 (6): 927–941. doi:10.1016/j.dsr.2006.01.013.

Bai, X., Z. Liu, X. Li, Z. Chen, J. Hu, Z. Sun, and J. Zhu. 2013. "Observations of High-Frequency Internal Waves in the Southern Taiwan Strait." *Journal of Coastal Research* 292: 1413–1419. doi:10.2112/JCOASTRES-D-12-00141.1.

Baines, P. G. 1982. "On Internal Tide Generation Models." *Deep Sea Research Part A. Oceanographic Research Papers* 29: 307–338. doi:10.1016/0198-0149(82)90098-X.

Bakhanov, V. V., and L. A. Ostrovsky. 2002. "Action of Strong Internal Solitary Waves on Surface Waves." *Journal of Geophysical Research* 107 (C10): 3139. doi:10.1029/2001JC001052.

Buijsman, M. C., Y. Kanarska, and J. C. McWilliams. 2010. "On the Generation and Evolution of Nonlinear Internal Waves in the South China Sea." *Journal of Geophysical Research* 115: C02012. doi:10.1029/2009JC005275.

Carnes, M. R. 2009. *Description and Evaluation of GDEM-V 3.0.*, *Naval Research Laboratory Report*. NRL/MR/7330-09-9165. Washington, DC: Naval Research Laboratory.

da Silva, J. C. B., A. L. New, and A. Azevedo. 2007. "On the Role of SAR for Observing Local Generation of Internal Solitary Waves off the Iberian Peninsula." *Canadian Journal of Remote Sensing* 33: 388–403. doi:10.5589/m07-041.

da Silva, J. C. B., A. L. New, and J. M. Magalhaes. 2009. "Internal Solitary Waves in the Mozambique Channel: Observations and Interpretation." *Journal of Geophysical Research Ocean* 114: C05001. doi:10.1029/2008JC005125.

da Silva, J. C. B., A. L. New, M. A. Srokosz, and T. J. Smyth. 2002. "On the Observability of Internal Tidal Waves in Remotely-Sensed Ocean Colour Data." *Geophysical Research Letters* 29: 1569. doi:10.1029/2001GL013888.

Djordjevic, V. D., and L. G. Redekopp. 1978. "The Fission and Disintegration of Internal Solitary Waves Moving over Two-Dimensional Topography." *Journal of Physical Oceanography* 8: 1016–1024. doi:10.1175/1520-0485(1978)008<1016:TFADOI>2.0.CO;2.

Du, T., Y. H. Tseng, and X. H. Yan. 2008. "Impacts of Tidal Currents and Kuroshio Intrusion on the Generation of Nonlinear Internal Waves in Luzon Strait." *Journal of Geophysical Research* 113: C08015. doi:10.1029/2007JC004294.

Egbert, G. D., and S. Y. Erofeeva. 2002. "Efficient Inverse Modeling of Barotropic Ocean Tides." *Journal of Atmospheric and Oceanic Technology* 19: 183–204. doi:10.1175/1520-0426(2002)019<0183:EIMOBO>2.0.CO;2.

Fu, K. H., Y. H. Wang, L. St. Laurent, H. Simmons, and D. P. Wang 2012. "Shoaling of Large-Amplitude Nonlinear Internal Waves at Dongsha Atoll in the Northern South China Sea." *Continental Shelf Research* 37. doi:10.1016/j.csr.2012.01.010.

Gerkema, T., and J. T. F. Zimmerman. 2008. *An Introduction to Internal Waves*. Lecture notes, 207. Texel: Royal NIOZ.

Guo, C., and X. Chen. 2014. "A Review of Internal Solitary Wave Dynamics in the Northern South China Sea." *Progress in Oceanography* 121: 7–23. doi: 10.1016/j.pocean.2013.04.002.

Guo, P., W. Fang, C. Liu, and F. Qiu. 2012. "Seasonal Characteristics of Internal Tides on the Continental Shelf in the Northern South China Sea." *Journal of Geophysical Research* 117: C04023. doi:10.1029/2011JC007215.

Jackson, C. R. 2007. "Internal Wave Detection Using the Moderate Resolution Imaging Spectroradiometer (MODIS)." *Journal of Geophysical Research* 112: C11012. doi:10.1029/2007JC004220.

Jackson, C. R. 2009. "An Empirical Model for Estimating the Geographic Location of Nonlinear Internal Solitary Waves." *Journal of Atmospheric and Oceanic Technology* 26: 2243–2255. doi:10.1175/2009JTECHO638.1.

Jiang, Y., F. Chai, Z. Wan, X. Zhang, and H. Hong. 2011. "Characteristics and Mechanisms of the Upwelling in the Southern Taiwan Strait: A Three-Dimensional Numerical Model Study." *Journal of Oceanography* 67: 699–708. doi:10.1007/s10872-011-0080-x.

Klymak, J. M., M. H. Alford, R. Pinkel, R. C. Lien, Y. J. Yang, and T. Y. Tang. 2011. "The Breaking and Scattering of the Internal Tide on a Continental Slope." *Journal of Physical Oceanography* 41: 926–945. doi:10.1175/2010JPO4500.1.

Klymak, J. M., R. Pinkel, C. T. Liu, A. K. Liu, and L. David. 2006. "Prototypical Solitons in the South China Sea." *Geophysical Research Letters* 33: L11607. doi:10.1029/2006GL025932.

Li, X., C. R. Jackson, and W. G. Pichel. 2013. "Internal Solitary Wave Refraction at Dongsha Atoll, South China Sea." *Geophysical Research Letters* 40: 3128–3132. doi:10.1002/grl.50614.

Li, X., Z. Zhao, Z. Han, and L. Xu. 2008. "Internal Solitary Waves in the East China Sea." *Acta Oceanologica Sinica* 27: 51–59.

Li, X., Z. Zhao, and W. G. Pichel. 2008. "Internal Solitary Waves in the Northwestern South China Sea Inferred from Satellite Images." *Geophysical Research Letters* 35: L13605. doi:10.1029/2008GL034272.

Lien, R. C., T. Y. Tang, M. H. Chang, and E. A. D'Asaro. 2005. "Energy of Nonlinear Internal Waves in the South China Sea." *Geophysical Research Letters* 32: L05615. doi:10.1029/2004GL022012.

Liu, A. K., Y. S. Chang, M.-K. Hsu, and N. K. Liang. 1998. "Evolution of Nonlinear Internal Waves in the East and South China Seas." *Journal of Geophysical Research* 103 (C4): 7995–8008. doi:10.1029/97JC01918.

Lozovatsky, I., Z. Liu, H. Fernando, J. Armengol, and E. Roget. 2012. "Shallow Water Tidal Currents in Close Proximity to the Seafloor and Boundary-Induced Turbulence." *Ocean Dynamics* 62: 177–191. doi:10.1007/s10236-011-0495-3.

Magalhaes, J. M., and J. C. B. da Silva. 2012. "SAR Observations of Internal Solitary Waves Generated at the Estremadura Promontory off the West Iberian Coast." *Deep Sea Research Part I: Oceanographic Research Papers* 69: 12–24. doi:10.1016/j.dsr.2012.06.002.

Merrifield, M. A., and P. E. Holloway. 2002. "Model Estimates of M_2 Internal Tide Energetics at the Hawaiian Ridge." *Journal of Geophysical Research* 107 (C8): 3179. doi:10.1029/2001JC000996.

Mitnik, L., W. Alpers, K. S. Chen, and A. J. Chen. 2000. "Manifestation of Internal Solitary Waves on ERS SAR and SPOT Images: Similarities and Differences." *Proceedings of the 2000 International Geoscience and Remote Sensing Symposium (IGARSS'00)* 5: 1857–1859.

Muacho, S., J. C. B. da Silva, V. Brotas, and P. B. Oliveira. 2013. "Effect of Internal Waves on Near-Surface Chlorophyll Concentration and Primary Production in the Nazaré Canyon (West of the Iberian Peninsula)." *Deep Sea Research Part I: Oceanographic Research Papers* 81: 89–96. doi:10.1016/j.dsr.2013.07.012.

Niwa, Y., and T. Hibiya. 2004. "Three-Dimensional Numerical Simulation of M_2 Internal Tides in the East China Sea." *Journal of Geophysical Research* 109: C04027. doi:10.1029/2003JC001923.

Pan, X., G. T. F. Wong, F.-K. Shiah, and T.-Y. Ho. 2012. "Enhancement of Biological Productivity by Internal Waves: Observations in the Summertime in the Northern South China Sea." *Journal of Oceanography* 68: 427–437. doi:10.1007/s10872-012-0107-y.

Sherwin, T. J., V. I. Vlasenko, N. Stashchuk, D. R. G. Jeans, and B. Jones. 2002. "Along-Slope Generation as an Explanation for Some Unusually Large Internal Tides." *Deep Sea Research Part I: Oceanographic Research Papers* 49: 1787–1799. doi:10.1016/S0967-0637(02)00096-1.

Vázquez, A., S. Flecha, M. Bruno, D. Macías, and G. Navarro. 2009. "Internal Waves and Short-Scale Distribution Patterns of Chlorophyll in the Strait of Gibraltar and Alborán Sea." *Geophysical Research Letters* 36: L23601. doi:10.1029/2009GL040959.

Vlasenko, V., C. Guo, and N. Stashchuk. 2012. "On the Mechanism of A-Type and B-Type Internal Solitary Wave Generation in the Northern South China Sea." *Deep Sea Research Part I: Oceanographic Research Papers* 69: 100–112. doi:10.1016/j.dsr.2012.07.004.

Wald, L., and J. M. Monget. 1983. "Sea Surface Winds from Sun Glitter Observations." *Journal of Geophysical Research* 88: 2547–2555. doi:10.1029/JC088iC04p02547.

Zhao, Z., and M. H. Alford. 2006. "Source and Propagation of Internal Solitary Waves in the Northeastern South China Sea." *Journal of Geophysical Research* 111: C11012. doi:10.1029/2006JC003644.

Zhao, Z., V. Klemas, Q. Zheng, and X. H. Yan. 2004. "Remote Sensing Evidence for Baroclinic Tide Origin of Internal Solitary Waves in the Northeastern South China Sea." *Geophysical Research Letters* 31: L06302. doi:10.1029/2003GL019077.

Zheng, Q., Y. T. Song, H. Lin, X. Hu, J. Meng, and D. Wang. 2008. "On Generation Source Sites of Internal Waves in the Luzon Strait." *Acta Oceanologica Sinica* 27: 38–50.

Zheng, Q., R. D. Susanto, C. R. Ho, Y. T. Song, and Q. Xu. 2007. "Statistical and Dynamical Analyses of Generation Mechanisms of Solitary Internal Waves in the Northern South China Sea." *Journal of Geophysical Research* 112: C03021. doi:10.1029/2006JC003551.